10

All-Dielectric Nanophotonic Structures: Exploring the Magnetic Component of Light

B. Hopkins*, A. E. Miroshnichenko, and Y. S. Kivshar

Nonlinear Physics Centre, Australian National University, Canberra 2601, Australia *ben.hopkins@anu.edu.au

Abstract. We discuss nanophotonic structures composed of high-index dielectric nanoparticles and present several basic approaches for numerical study of their collective optical response. We also provide comparison on the collective optical properties of dielectric and plasmonic structures, and review experimental demonstrations of Fano resonances in all-dielectric nanoparticle oligomers.

10.1 Introduction

Recent progress in nanophotonics is often associated with the study of plasmonic structures that have enabled enhanced near-field effects at the nanoscale and control over far-field scattering. However, a new branch of nanophotonics has emerged through the manipulation of strong optically-induced Mie-type electric and magnetic resonances in dielectric and semiconductor nanoparticles with high refractive index. High-index resonant nanoparticles offer many advantages over their plasmonic counterparts in terms of reduced dissipative losses, low heating, and the resonant enhancement of both electric and magnetic fields [1–3]. The coexistence of electric and magnetic resonances has also enabled effective realization of Kerker's conditions [4] for reflectionless scattering by using individual dielectric nanoparticles [5–9], a development that subsequently allows various new phenomena for manipulation of directional light scattering [10–12] and optical nano-antenna applications [13–15]. This Chapter summarizes several basic numerical approaches applied to the analysis of all-dielectric nanophotonic structures, while also comparing our results with those of plasmonic structures, and their functionalities. Within this scope, we put significant emphasis on one particular area has garnered significant attention in recent years: the study of Fano resonances in nanoparticle oligomers and cluster structures [16,17]. While the aforementioned directionality of single dielectric nanoparticles can be considered as an effect of interference in the

scattering along particular directions, Fano resonances correspond to a resonant interference in the *total* scattering of an object. Yet, these two phenomena will become interdependent if an all-dielectric nanoparticle oligomer were to exhibit Fano resonances, thereby presenting a new layer to scattering phenomena at the nanoscale. In this regard, Fano interference has been predominantly described for specific plasmonic oligomers, where a directly-excited superradiant mode interferes destructively with an indirectly-excited "dark mode" (or trapped mode). In essence, the near-field interaction, or *hybridization*, of plasmons provides a coupling channel between different resonant subsystems of a plasmonic nanostructure. This description can then resemble a classical oscillator model for Fano resonances [18, 19], where a driven oscillator is able to resonantly couple its external driving force into an adjacent oscillator. Yet, it is less clear how to apply this description when the separation of a collective system into distinct resonant subsystems is highly ambiguous, or simply not possible. Further, it was then predicted that Fano resonances should also occur in all-dielectric symmetric oligomers [63], despite the absence of plasmon hybridization between nanoparticles. The formal treatment presented herein, considers Fano resonances instead from the resonances of the collective system, *i.e.* without separation into resonant subsystems. This approach demonstrates a common mechanism underlying the physics of Fano resonances in both plasmonic and all-dielectric oligomers, attributing their existence to the fact that the eigenmodes of collective oligomers are not orthogonal and that, therefore, they can interfere with each other. This also establishes why Fano resonances can be realized in completely symmetric oligomers excited by normal incidence plane waves, without involving additional complexity into the system.

The structure of the chapter will therefore follow a path from the modelling of dielectric nanoparticle systems in Section 10.2, into the general model for collective resonances and Fano resonances using an eigenmode description for plasmonic and dielectric nanoparticle oligomers in Section 10.3. We then conclude by reviewing the recent experimental developments in producing Fano resonances in dielectric nanoparticle oligomers in Section 10.4.

10.2 Modeling All-Dielectric Nanoparticle Systems

10.2.1 Maxwell's Equations for Nanophotonics

Physically, electromagnetism describes retarded forces between charges. Electric and magnetic fields are defined as heralds of linear and rotational force on charges, a basis that has been historically necessary, or at least convenient, because it corresponds to the way natural materials respond. Indeed, atoms and other neutral compositions of charged matter dominantly behave as per electric and magnetic dipoles: oscillating charges and circulating currents. Material then arises when defining regions of closely packed electric and magnetic

dipoles with homogenized volumes of electric and magnetic dipole densities, two densities which we refer to as *permittivity* and *permeability*. Homogenization, as such, inherently corresponds to material as found in nature. However, this macroscopic description need not align with the advent of metamaterials, nanoantennas, and complex structured media generally [20]. Macroscopic assemblies of subwavelength *meta-atoms* will not necessarily respond to fields as per linear or rotational movement of charge; the constituent point sources in such a homogenized material are not necessarily electric or magnetic dipoles. Even compact arrangements of coupled dipolar nanoparticles can collectively exhibit higher-order optical behavior on a subwavelength scale [21]. Therefore, underlying the rapid development of complex nanophotonic structures is a need to re-evaluate how we understand the optical properties of complex structured objects and media. The development of all-dielectric nanostructures is one area of investigation that now demands a detailed understanding on the limits of complex optical materials. This is ultimately because simple nanostructures made from a high-index dielectric material are able to exhibit both electric and magnetic response, including magnetic resonances that are of similar magnitude or even stronger than the electric dipole resonances of plasmonic nanoparticles, as is seen in Figure 10.1. This figure also demonstrates how the reduced material loss of silicon leads to less damping in the resonances of silicon nanoparticles, thereby producing higher Q-factors when compared to plasmonic counterparts. Generalization of the electric and magnetic single particle response for arbitrary, high refractive index, dielectric materials also translates this behavior across a large spectrum, owing to the scaling properties of the resonances with refractive index and nanoparticle size [3].

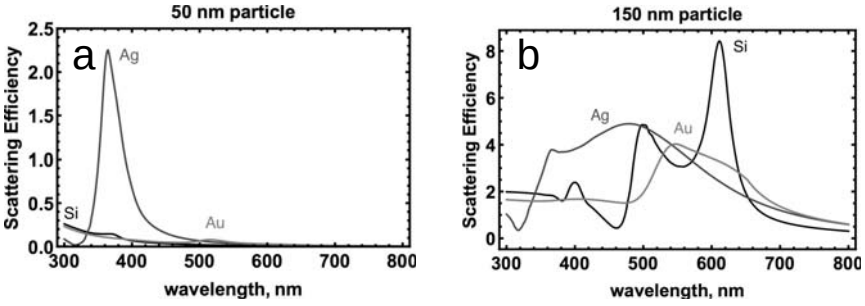

Fig. 10.1. Comparison of the scattering cross-sections of gold, silver and silicon nanoparticles of the same geometrical sizes: (a) diameter 50 nm, and (b) diameter 150 nm. These results demonstrate that in addition to a new type of resonances dielectric particles scatter light more efficiently than plasmonic ones for larger sizes. Produced after A. I. Kuznetsov [22].

The seemingly small change of having both electric and magnetic dipole resonances can have dramatic effects on the scattering behavior of single nanostructures [4, 23, 24], but also collective nanoparticle clusters [25, 26] and arrays [27–30]. In this Chapter, we address the challenge of understanding complex dielectric nanostructures firstly in terms of free currents and polarization currents, because they are the underlying physical sources of fields within any arbitrary system, and thereby encapsulate its complete optical characteristics. Secondly, we present the dipole model as a practical simplification that allows direct investigation of the dominant resonances of compact nanoparticle systems. This two-model approach is used for understanding the physics of nanoparticle cluster geometries consisting of high-index dielectric nanoparticles, and reconciling the simultaneous interplay of electric and magnetic fields in these scattering systems. In doing so, we aim to establish a platform on which nanoscale designs can be reliably manipulated to capitalize on the interaction between dielectric nanoparticles and the magnetic field in light.

10.2.2 Radiation by Internal Current Distributions

We begin our scattering analysis of linear optical systems by acknowledging that any arbitrary time-varying electric and magnetic fields can be described as a distribution of harmonic fields in a Fourier series representation. Furthermore, for monochromatic response, there is no particular need to recognize the distinction between free current and polarization current, given conductivity $\bar{\sigma}$ and susceptibility $\bar{\chi}$ can be incorporated into an effective permittivity $\bar{\epsilon}$ that relates electric field $\mathbf{E}$ to a *total* electric current $\mathbf{J}$.

$$\bar{\epsilon} \equiv (\bar{\chi} + 1)\epsilon_0 - \frac{\bar{\sigma}}{i\omega} \quad \Rightarrow \quad \mathbf{J}(\mathbf{r})e^{-i\omega t} = -i\omega\big(\bar{\epsilon}(\mathbf{r}) - \epsilon_0\big)\mathbf{E}(\mathbf{r})e^{-i\omega t} \tag{10.1}$$

There is also the simplification that most optical materials have a negligible difference in permeability compared to their respective background medium, allowing us to neglect the radiation from any magnetization current. As such, the field $\mathbf{E_s}$ scattered from an arbitrary structure can be described by radiation from a distribution of electric current, and can be expressed in terms of dyadic Green's functions [31].

$$\mathbf{E_s}(\mathbf{r}) = i\omega\mu_0 \int_V \bar{G}_0(\mathbf{r}, \mathbf{r}')\mathbf{J}(\mathbf{r}')\ \mathrm{d}{\mathbf{r}'}^3 \tag{10.2}$$

where k is the wavenumber, ω is the angular frequency, ϵ_0 and μ_0 are the permittivity and permeability of the background medium, and V is the volume of the scattering object, which we assume here to be finite. The remaining part of the expression is the free space dyadic Green's function $\bar{G}_0$:

$$\bar{G}_0(\mathbf{r}, \mathbf{r}') = \mathrm{P.V.}\left(\bar{\mathrm{I}} + \frac{1}{k^2}\boldsymbol{\nabla}\boldsymbol{\nabla}\right)\frac{e^{ikR}}{4\pi R} - \bar{\mathrm{L}}\frac{\delta(\mathbf{r} - \mathbf{r}')}{k^2} \tag{10.3}$$

where $R = |\mathbf{r} - \mathbf{r}'|$, the P.V. implies a principal value exclusion of $\mathbf{r}' = \mathbf{r}$ when performing the integration in Equations 10.1 and 10.4, and $\bar{\mathrm{L}}$ is the source dyadic necessary to account for the shape of this exclusion [31]. Notably, we can then use this expression for the scattered field to find the current induced by an external electric field $\mathbf{E_0}$. In particular, using Equation 10.1, the current can found from the total interal field $\mathbf{E} = \mathbf{E_0} + \mathbf{E_s}$, producing the following relation between the induced field and the external field:

$$-i\omega\big(\bar{\epsilon}(\mathbf{r}) - \epsilon_0\big)\,\mathbf{E}_0(\mathbf{r}) = \mathbf{J}(\mathbf{r}) - \frac{k^2}{\epsilon_0}\big(\bar{\epsilon}(\mathbf{r}) - \epsilon_0\big)\int_V \bar{G}_0(\mathbf{r},\mathbf{r}')\mathbf{J}(\mathbf{r}')\;\mathrm{d}\mathbf{r}'^3 \qquad (10.4)$$

As such, Equation 10.4 and Equation 10.2 will completely describe the currents induced and fields radiated, respectively, by any arbitrary finite structure in the absence of magnetization. This is a comprehensive description of general scattering systems, and is therefore useful for finding broad analytical conclusions as a result of geometry. Below, we will use it to discuss the relation between far-field interference features and the nonorthogonality of eigenmodes for the induced current. It is, however, highly nontrivial to obtain a general, excitation-independent, modal solution for Equation 10.4 for even very simple geometries, plainly because the model inherently describes the complete dynamics of a given object's scattering, encapsulating all resonances, irrespective of their magnitude. One existing numerical approach for calculating the general scattering properties of any arbitrary object from the resonances of surface current distributions is implemented through the *OpenModes* software, which deals with complexity by searching for only a subset of the complex frequency resonances [32]. Here, however, we will focus on arrangements of simple nanoparticles, so-called *oligomers*, which utilize the coupling between nanoparticles, rather than nanoparticle geometry, to produce complex optical features such as Fano resonances [25, 33] and near-field control [34, 35]. For these nanoparticle oligomers, we are able to restrict our analysis to the dominant optical properties of the collective geometry by only considering the dominant optical response of the individual nanoparticles. In particular, the model that will be used extensively throughout the remainder of this Chapter is to consider only the dipole-order responses of individual nanoparticles. As we will show, this approach suffers from only minor limitations in accuracy while offering dramatic simplifications in modal analysis.

10.2.3 Dipole Models

The constituent nanoparticles of oligomers are, in general, of simple geometry and subwavelength in size, which implies that their individual optical responses can be entirely described in terms of resonant dipole moments [1, 36]. We will begin in the simpler case of plasmonic nanoparticles, where the individual nanoparticle response is dominantly an electric dipole, and we can therefore use the dipole approximation [37] to describe the optical properties

of the oligomer. In particular, each nanoparticle's electric dipole moment ($\mathbf{p}_i$) is related to the externally-applied electric field ($\mathbf{E_0}$) as:

$$\mathbf{p}_i = \alpha_E^{(i)} \epsilon_0 \mathbf{E_0}(\mathbf{r}_i) + \alpha_E^{(i)} k^2 \sum_{j \neq i} \bar{G}_0(\mathbf{r}_i, \mathbf{r}_j) \cdot \mathbf{p}_j \tag{10.5}$$

Here, $\alpha_{E,i}$ is the electric dipole polarizability of the i^{th} particle and we can write the effect of $\bar{G}_0$ more explicitly as:

$$\bar{G}_0(\mathbf{r}', \mathbf{r}) \cdot \mathbf{p} = \frac{e^{ikR}}{4\pi R} \left[\left(1 + \frac{i}{kR} - \frac{1}{k^2 R^2}\right) \mathbf{p} - \left(1 + \frac{3i}{kR} - \frac{3}{k^2 R^2}\right) (\mathbf{n} \cdot \mathbf{p})\, \mathbf{n} \right] \tag{10.6}$$

where $\mathbf{n}$ is the unit vector pointing from $\mathbf{r}$ to $\mathbf{r}'$. The expression in Equation 10.5 forms a matrix equation of rank $3N$, where N is the number of dipoles, and it can be solved for an arbitrary excitation as per an ordinary matrix equation. In Figure 10.2a, we present the validity of this model for a symmetric trimer arrangement of gold nanospheres, where the electric dipole polarizabilities of the nanospheres are calculated through a_1 scattering coefficients from Mie theory [38, 39], *c.f.* Equation 10.7. Even with very small gaps between the spheres, the dipole model offers an accurate prediction of the trimer's response, with the exception of that coming from the single particle electric quadrupole response. However, the situation becomes notably different when we utilize high-index dielectric nanoparticles. Simple dielectric nanospheres will also exhibit a magnetic dipole resonance in addition to an electric dipole resonance. Indeed, we can express the electric and magnetic dipole polarizabilities in terms of the a_1 and b_1 scattering coefficients, which are known from Mie theory for the case of spheres [38, 39].

$$\alpha_E = \frac{6i\pi a_1}{k^3}\,, \qquad \alpha_H = \frac{6i\pi b_1}{k^3} \tag{10.7}$$

To this end, the dipole model in Equation 10.5 can then be extended to include both electric and magnetic dipoles [36]

$$\mathbf{p}^{(i)} = \alpha_E^{(i)} \epsilon_0 \mathbf{E_0}(\mathbf{r}_i) + \alpha_E^{(i)} k^2 \left(\sum_{j \neq i} \bar{G}_0(\mathbf{r}_i, \mathbf{r}_j) \cdot \mathbf{p}^{(j)} - \frac{1}{c_0} \nabla \times \bar{G}_0(\mathbf{r}_i, \mathbf{r}_j) \cdot \mathbf{m}^{(j)} \right) \tag{10.8a}$$

$$\mathbf{m}^{(i)} = \alpha_H^{(i)} \mathbf{H_0}(\mathbf{r}_i) + \alpha_H^{(i)} k^2 \left(\sum_{j \neq i} \bar{G}_0(\mathbf{r}_i, \mathbf{r}_j) \cdot \mathbf{m}^{(j)} + c_0 \nabla \times \bar{G}_0(\mathbf{r}_i, \mathbf{r}_j) \cdot \mathbf{p}^{(j)} \right) \tag{10.8b}$$

where $\mathbf{p}^{(i)}$ ($\mathbf{m}_i$) is the electric (magnetic) dipole moment of the i^{th} particle, $\bar{G}_0(\mathbf{r}_i, \mathbf{r}_j)$ is the free space dyadic Green's function between the i^{th} and j^{th} dipole, $\alpha_E^{(i)}$ ($\alpha_H^{(i)}$) is the electric (magnetic) dipole polarizability of the i^{th} particle, c_0 is the speed of light in free-space and k is the free-space wavenumber. The extra cross-coupling terms are given according to:

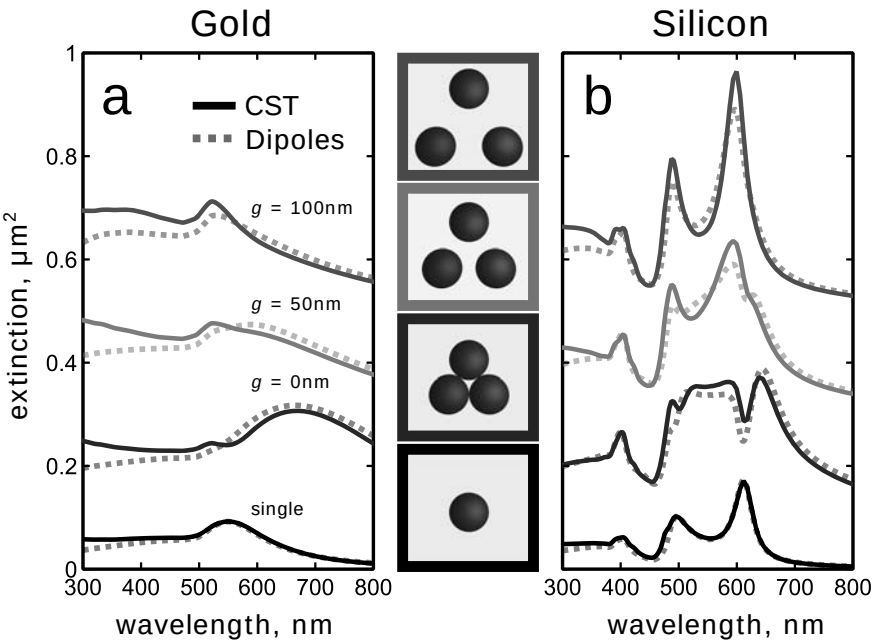

Fig. 10.2. A comparison of the extinction cross-section calculated using CST Microwave Studio with that calculated using the dipole model in Equation 10.8. Calculations are for 150 nm nanospheres made of (a) gold and (b) silicon, when arranged as symmetric trimers with varying separation g between nanoparticles.

$$\nabla \times \bar{G}_0(\mathbf{r}', \mathbf{r}) \cdot \mathbf{p} = \frac{e^{ikR}}{4\pi R}\left(1 + \frac{i}{kR}\right)\mathbf{n} \times \mathbf{p} \tag{10.9}$$

Notably, Equation 10.5 is the discrete equivalent to the continuous current distribution model in Equation 10.4, and in Equation 10.8 it is extended to account for magnetization currents in addition to polarization currents. In other words, the magnetic dipoles introduced into Equation 10.8 behave as per sources of magnetization current. This description of circulating current in a nanoparticle is, at least macroscopically, indistinguishable to a source of true magnetization that derives from material permeability. Indeed, this can be understood due to the fact that, regarding atoms in natural materials, permeability was originally defined to describe circulating currents. This is analogous to circulating polarization current as per Equation 10.1, and a high-index dielectric nanoparticle remains smaller than the resonant wavelength, even if much larger than either atoms or molecules. As such, dielectric nanoparticles allow a straightforward avenue to access effective material properties with both permittivity and permeability. However, we previously mentioned that a key advantage of nanostructures is to go beyond conventional materials. In this regard, we simply need to acknowledge that a single nanoparticle will

rarely act in isolation: it radiates and couples with other nearby nanoparticles to form collective modes, and the individual nanoparticles no longer respond proportionally to the applied electric and magnetic fields as per permittivity and permeability. In the next section we investigate such collective optical responses rigorously by presenting an eigenmode approach for describing the optical responses of coupled nanoparticle scattering systems.

10.3 Eigenmodes of Nanoparticle Oligomers

10.3.1 Resonances, Polarizability, and Eigenmodes

One of the most important properties of nanoscale structures is their resonant response. Thus, it is important to understand conditions of the resonance in order to tailor it toward some given application, be it electric or magnetic field localization, directionality, chiral resonances, or any number of other potential applications. In this regard, the majority of quantitative approaches to characterize a resonance rely on a multipolar decomposition of a given resonance. There are two approaches to get such a multipolar decomposition: project the scattered field onto spherical harmonics to obtain a spherical multipole decompositions, or project the internal current and charge distributions onto Cartesian multipoles (and their various correction factors) to obtain a Cartesian multipole decomposition [40–42]. Such decompositions can then be used to define polarizabilities, or impedances, for each multipolar dimension [43]. However, these polarizabilities, and the multipolar decompositions more generally, are inherently dependent on the choice of origin when performing the decomposition. As such, they ultimately remain a non-unique basis for the scattering responses, where any given multipole is not necessarily fully-representative of the given resonance. This can lead to a large number of multipoles being necessary to describe a single resonance. Furthermore, while there is an intuitive choice of origin for simple nanostructures, it can be much less obvious for complex nanostructures or arrangements of nanoparticles, including nanoparticle oligomers. Equivalently, the multipole decomposition may simply not align well with the resonances of a given object. These same issues can impact other existing analytical tools in nanophotonics, such as the T-matrix method, because it relies on the same spherical multipole decomposition of scattered fields. Indeed, to understand the resonances of a system more fundamentally, and in a way that is independent of the choice of origin, we can instead consider the eigenmodes of the electric current system in the presence of a driving field. Moreover, Eq. 10.4 has an associated eigenmode equation, where an eigenmode $|v\rangle$ has a current distribution $\mathbf{J}_v$ and eigenvalue λ_v that satisfies:

$$i\omega\lambda_v\mathbf{J}_v(\mathbf{r}) = -\left(\bar{\epsilon}(\mathbf{r}) - \epsilon_0\right)^{-1}\mathbf{J}_v(\mathbf{r}) + \frac{1}{\epsilon_0}\int_V \bar{G}_0(\mathbf{r},\mathbf{r}')\mathbf{J}_v(\mathbf{r}')\,\mathrm{d}\mathbf{r}'^3 \qquad (10.10)$$

These eigenvalues and eigenmodes represent an origin-independent basis of polarizabilities or impedances, and the associated stable current distributions, respectively. Furthermore, at any single wavelength, the set of eigenmodes represents the *only* basis for the optical response where each basis vector represents a current distribution that is subject to energy conservation in isolation. In a mathematical sense, the real component of the eigenvalue must be greater than zero to satisfy passivity, or must be less than zero to be active (refer to Equation 10.18), where *active* means inputting net energy into the system and *passive* simply refers to being not active. The final characteristic to recognize is that the complex frequency where an eigenvalue becomes zero corresponds to a self-sustaining current distribution, otherwise recognized as a resonance of the system. In fact, given the eigenmodes will almost always form a complete and linearly-independent basis, *every* such self-sustaining resonance must be associated with at least one zero eigenvalue. In summary, the eigenmode decomposition obtains a complete set of underlying resonances at *complex* frequencies, while also providing the only complete set of necessarily-passive basis vectors at *real* frequencies, and further connecting these two physical attributes together in a consistent and origin-independent modal framework. A basis of eigenmodes thereby provides both mathematical and physical insight into the underlying optical response of any finite scattering system. As we will address in the next section, there is an added significance that the current model here contains loss and is thereby generally non-Hermitian, meaning eigenmodes need not be orthogonal. However, the specific excitation of each eigenmode in the current model can still be found through the impact of reciprocity on the eigenmodes of any arbitrary system. Moreover, Onsager's Reciprocity requires that the dyadic Green's function and permittivity tensor be symmetric [44], albeit complex and not necessarily Hermitian.

$$\bar{G}_0(\mathbf{r},\mathbf{r}') = \bar{G}_0(\mathbf{r}',\mathbf{r}), \quad \bar{G}_0 = \bar{G}_0^T, \quad \bar{\epsilon} = \bar{\epsilon}^T \tag{10.11}$$

Due to this symmetry, it is possible to write the overall operator of the eigenvalue equation (Eq. 10.10) as a matrix in the normal form shown by Gantmacher [45]. This then shows that nondegenerate eigenmodes are orthogonal under unconjugated projections [46]

$$\int_V \mathbf{J}_v(\mathbf{r}) \cdot \mathbf{J}_w(\mathbf{r}) \, \mathrm{dr}^3 = 0\,, \quad \text{when } \lambda_v \neq \lambda_w \tag{10.12}$$

This pseudo-orthogonality of eigenmodes makes the excitation of any eigenmode determined through unconjugated dot products between the eigenmode and a driving field, analogous to the more familiar use of true complex projections when finding the excitation of orthogonal eigenmodes. As such, despite eigenmodes being nonorthogonal, any given eigenmode's excitation is not dependent on the excitations of other eigenmodes: it is determined entirely by the given eigenmode's current distribution and the driving field. Turning now to our consideration of nanoparticle oligomers, this conclusion carries over to

the eigenmodes of systems made from purely electric dipoles. An eigenmode $|v\rangle$ having electric dipoles $\mathbf{p}_v$ will satisfy Eq. 10.5 as:

$$\mathbf{p}_v^{(i)} = \alpha_E^{(i)} \epsilon_0 \lambda_v \mathbf{p}_v^{(i)} + \alpha_E^{(i)} \sum_{j \neq i} k^2 \bar{G}_0(\mathbf{r}_i, \mathbf{r}_j) \cdot \mathbf{p}_v^{(j)} \tag{10.13}$$

This relationship between this dipole model and the current distribution model is not surprising given polarization and current are related as per Equation 10.1, where free currents are described in terms of polarization current. Indeed, beyond accounting for the factor of $i\omega$ and the source dyadic $\bar{L}$, the dipole model is the same as the current model when the current distribution is described by a countable set of Dirac delta functions.

However, when introducing magnetic dipoles, we are describing the magnetic response of dielectric nanoparticles as magnetization. Because of this, eigenmodes will be simultaneously constructed of both polarization and magnetization, where each has different units. To address this difference of units, an initial approach was to separate the eigenmodes of electric and magnetic dipoles by introducing a term that describes the driving of electric dipoles by an applied magnetic field, and the driving of magnetic dipoles by an applied electric field [21]. In effect, this approach finds the eigenmodes of either the electric *or* the magnetic dipole systems, and their polarizabilities (eigenvalues), irrespective of the effect they have on the other dipole system. This description will necessarily have cross terms accounting for interaction between the electric and magnetic eigenmodes, analogous to tensor bianisotropic polarizabilities. However, while this is a full description of the dipole system, and it provides information on the resonances of electric and magnetic systems in the presence of each other, it *does not* describe the simultaneous stable oscillations of both the electric *and* magnetic dipoles, which are ultimately the resonances of the collective system. To consider the eigenmodes and resonances of the collective system, we must consider both electric and magnetic dipoles together. In this regard, it is necessary to introduce relative scaling between the electric and magnetic dipoles to maintain fixed units of polarizability for the resulting eigenvalues, and to also maintain the passivity of eigenmodes at real frequencies. Moreover, the magnetic dipoles can be scaled by a factor of ${c_0}^{-1}$, and the magnetic field by a factor of $\sqrt{\mu_0/\epsilon_0}$. An eigenmode $|v\rangle$, having electric dipoles $\mathbf{p}_v$ and magnetic dipoles $\mathbf{m}_v$, will satisfy the coupled electric and magnetic dipole model (Equation 10.8) as:

$$\lambda_v \, \mathbf{p}_v^{(i)} = (\bar{\alpha}_E^{(i)} \epsilon_0)^{-1} \mathbf{p}_v^{(i)} - \frac{k^2}{\epsilon_0} \Big(\bar{G}_0(\mathbf{r}_i, \mathbf{r}_j) \cdot \mathbf{p}_v^{(j)} + \nabla \times \bar{G}_0(\mathbf{r}_i, \mathbf{r}_j) \cdot [c_0^{-1} \mathbf{m}_v^{(j)}] \Big) \tag{10.14a}$$

$$\lambda_v \, [c_0^{-1} \mathbf{m}_v^{(i)}] = (\bar{\alpha}_H^{(i)} \epsilon_0)^{-1} [c_0^{-1} \mathbf{m}_v^{(i)}] - \frac{k^2}{\epsilon_0} \Big(\bar{G}_0(\mathbf{r}_i, \mathbf{r}_j) \cdot [c_0^{-1} \mathbf{m}_v^{(j)}] - \nabla \times \bar{G}_0(\mathbf{r}_i, \mathbf{r}_j) \cdot \mathbf{p}_v^{(j)} \Big) \tag{10.14b}$$

This expression describes a matrix equation for eigenmodes of the electric and magnetic dipole system describing N nanoparticles. The associated $6N \times 6N$ matrix will, notably, not be symmetric when there is non-negligible coupling between the electric and magnetic dipoles, and therefore the corresponding eigenmodes will not maintain the pseudo-orthogonality analogous to that in Equation 10.12 for currents. Nonetheless, it worth acknowledging that this practice of replacing circulating current with magnetization remains analogous to the practice used to define permeability for conventional materials. Therefore, the coupled electric and magnetic dipole model, including its resonances and their associated eigenmodes, should maintain the appropriate relationship to magnetic field to be the foundation for our analysis of all-dielectric nanoparticle oligomers.

10.3.2 Modal Interference and Fano Resonances

We begin by noting that both the current model and the dipole model describe open, radiative systems. As such, even in the absence of material loss, the system does still exhibit radiation losses and is generally, therefore, *non-Hermitian*. The immediate consequence of this non-Hermicity is that the eigenmodes we have defined in Equations 10.10, 10.13 and 10.14 are not necessarily orthogonal. To recognize the effect of this nonorthogonality, and its relation to the Fano resonances, we can refer to the extinction cross-section, which describes the total loss in a system. To not make any assumptions on the excitation field, we can construct extinction from the sum of the scattering and absorption cross-sections. The scattering cross-section can be calculated from the integral of the far-field scattered power, such as derived by Merchiers *et al.* [47] for the case of electric and magnetic dipoles.

$$\begin{aligned}\sigma_{\mathrm{s}} =& \frac{k}{{\epsilon_0}^2 I_0}\mathrm{Im}\Bigg[\sum_i \epsilon_0 {\mathbf{E_0}}^*(\mathbf{r}_i)\cdot\mathbf{p}_i + \epsilon_0\mu_0 {\mathbf{H_0}}^*(\mathbf{r}_i)\cdot\mathbf{m}_i \\ &+ \mathbf{p}_i^*\cdot\Big(\frac{ik^3}{6\pi} + (\bar{\alpha}_E^{(i)})^{-1}\Big)\mathbf{p}_i + \epsilon_0\mu_0\mathbf{m}_i^*\cdot\Big(\frac{ik^3}{6\pi} + (\bar{\alpha}_H^{(i)})^{-1}\Big)\mathbf{m}_i\Bigg] \end{aligned} \tag{10.15}$$

where I_0 is associated with the average intensity of the excitation such that it relates the area of a cross-section σ to the total power P as per $P = \frac{1}{2}\sqrt{\frac{\mu_0}{\epsilon_0}}\, I_0\, \sigma$. The absorption cross-section can be calculated from the closed surface integral of the total Poynting vector field around the scattering object, or by calculating the Ohmic losses of the internal electric and magnetic field [48].

$$\sigma_{\mathrm{a}} = \frac{-k}{{\epsilon_0}^2 I_0}\mathrm{Im}\Bigg[\mathbf{p}_i^*\cdot\Big(\frac{ik^3}{6\pi} + (\bar{\alpha}_E^{(i)})^{-1}\Big)\mathbf{p}_i + \epsilon_0\mu_0\mathbf{m}_i^*\cdot\Big(\frac{ik^3}{6\pi} + (\bar{\alpha}_H^{(i)})^{-1}\Big)\mathbf{m}_i\Bigg] \tag{10.16}$$

The extinction cross-section, as the sum of absorption and scattering, can then be written as:

$$\sigma_{\mathrm{e}} = \frac{k}{\epsilon_0 I_0} \mathrm{Im}\Big[\sum_i \mathbf{E_0}^*(\mathbf{r}_i) \cdot \mathbf{p}_i + \mu_0 \mathbf{H_0}^*(\mathbf{r}_i) \cdot \mathbf{m}_i \Big] \tag{10.17}$$

Notably, this is still the same expression as if we had used the Optical Theorem with plane wave excitation [47]. The equivalent expression for extinction in the current model in Equation 10.4, can be found by expressing a current distribution as an equivalent and infinite distribution of point dipoles [49].

$$\sigma_{\mathrm{e}} = \frac{1}{I_0} \sqrt{\frac{\mu_0}{\epsilon_0}}\, \mathrm{Re}\Big[\int_{V_s} \mathbf{E}_0^* \cdot \mathbf{J}\, \mathrm{d}^3 \Big] \tag{10.18}$$

From this expression, we acknowledge that an arbitrary applied field and the induced currents can be defined in terms of a linear superposition of the eigenmodes:

$$\mathbf{E}_0 = \sum_v a_v \lambda_v \mathbf{J}_v \quad \Rightarrow \quad \mathbf{J} = \sum_v a_v \mathbf{J}_v \tag{10.19}$$

We are then able to rewrite the total extinction (Equation 10.18) in terms of eigenmodes and eigenvalues. Moreover, we can divide the extinction into two contributions: *direct terms* that provide contributions to extinction from individual eigenmodes, and also *interference terms* coming from the overlap between different eigenmodes.

$$\sigma_{\mathrm{e}} = \frac{1}{I_0} \sqrt{\frac{\mu_0}{\epsilon_0}} \sum_v \Bigg(\underbrace{\mathrm{Re}[\lambda_v] \int_V |a_v|^2 |\mathbf{J}_v|^2 \, \mathrm{d}^3}_{\text{direct terms}} + \sum_{w \neq v} \underbrace{\mathrm{Re}\Big[a_v^* a_w \lambda_v^* \int_V \mathbf{J}_v^* \cdot \mathbf{J}_w \, \mathrm{d}^3 \Big]}_{\text{interference terms}} \Bigg) \tag{10.20}$$

The direct terms are always greater than zero due to the inscribed passivity of eigenmodes, and interference terms would notably all be zero for orthogonal eigenmodes. As we will now explain, the existence of nonzero interference terms, and thereby the presence of nonorthogonal eigenmodes, is required for Fano resonances to exist. Moreover, a given eigenmode's excitation, being the a_i coefficients of Equation (10.19), will be independent from the excitations of other eigenmodes - a conclusion directly from the pseudo-orthogonality in Equation 10.12. The only way an interaction between two or more eigenmodes affects the extinction cross-section is, therefore, through interference terms, meaning that Fano resonances must be described by the nonorthogonality of eigenmodes. This is indeed the conclusion of earlier works on the Fano resonances arising in nanoparticle oligomers [21,50], and is in good accordance with Fano resonances that have been proposed and observed to occur between modes that are directly driven by the incident field [51,52]. As an example, we consider heptamers made from gold nanospheres shown in Figure 10.3a. By performing an eigenmode decomposition of this system, we show the direct

terms of extinction coming from the dominant eigenmodes, in addition to the total extinction. This means the difference between total extinction and the sum of direct terms are the interference terms is coming from eigenmode overlap. For the case of the gold heptamer, we have a typical scenario of the Fano resonances: the overlap of a broad resonance and a sharp resonance, and coupling that leads to destructive interference. This gold heptamer thereby shows a classical example of a Fano resonance [16], where the interaction between resonances is coming from eigenmode nonorthogonality.

However, as seen in Figure 10.3b, the situation becomes dramatically more complicated for a silicon heptamer. The number of eigenmodes of this system is much higher, because of both the additional magnetic dipoles and because electric-magnetic dipole coupling (*c.f.* Equation 10.9) allows each dipole to be polarized parallel to the propagation direction [53]. The first consequence of this increased eigenmode count is that there are many more signatures of interference phenomena occurring across the extinction spectra. However, the second consequence is that we have to accept the formation of *exceptional points*. An exceptional point refers to a point degeneracy of two or more eigenvalues when their eigenmodes simultaneously become linearly dependent, subsequently corresponding to a reduction in the dimension of the span of eigenmodes [54–56]. Exceptional points can exist even in simple plasmonic and dielectric oligomer systems at complex frequencies [53], but can be expected to occur more regularly when there are more interacting eigenmodes. For the discussion here, we need to recognize that the excitation magnitudes of coalescing eigenmodes can diverge in the vicinity of an exceptional point, given a component of the driving field is gradually becoming orthogonal to the eigenmodes that span it. However, a full discussion of the properties of exceptional points will not be covered, and we have therefore attempted to divert attention away from the direct extinction terms of individual eigenmodes that diverge as they near exceptional points in Figure 10.3b. The reason we observe such features is likely because the number of eigenmodes that are excited by a normally-incident plane wave in a dielectric oligomer can be more than double that for a plasmonic oligomer. Assuming a normally-incident plane wave, the number of excitable eigenmodes in such rotationally-symmetric plasmonic oligomers is relatively contained: two degenerate pairs of eigenmodes for each ring of nanoparticles and one further pair if there is central nanoparticle [21]. On the other hand, the coupling between electric and magnetic dipoles in dielectric oligomers removes such eigenmode restrictions, making the number of excitable eigenmodes increase with the number of nanoparticles in each ring [53]. This means that even simple arrangements of dielectric nanoparticles can be used to achieve the behavior of more complicated plasmonic oligomers, an example of which will be investigated in the next section.

Finally, as an addendum, we should recognize that there is a degree of freedom in how to attribute extinction to each given eigenmode. In particular, rather than separating direct and interference terms as per Equation 10.20, Frimmer *et al.* [51] attributed the extinction associated with a given eigenmode

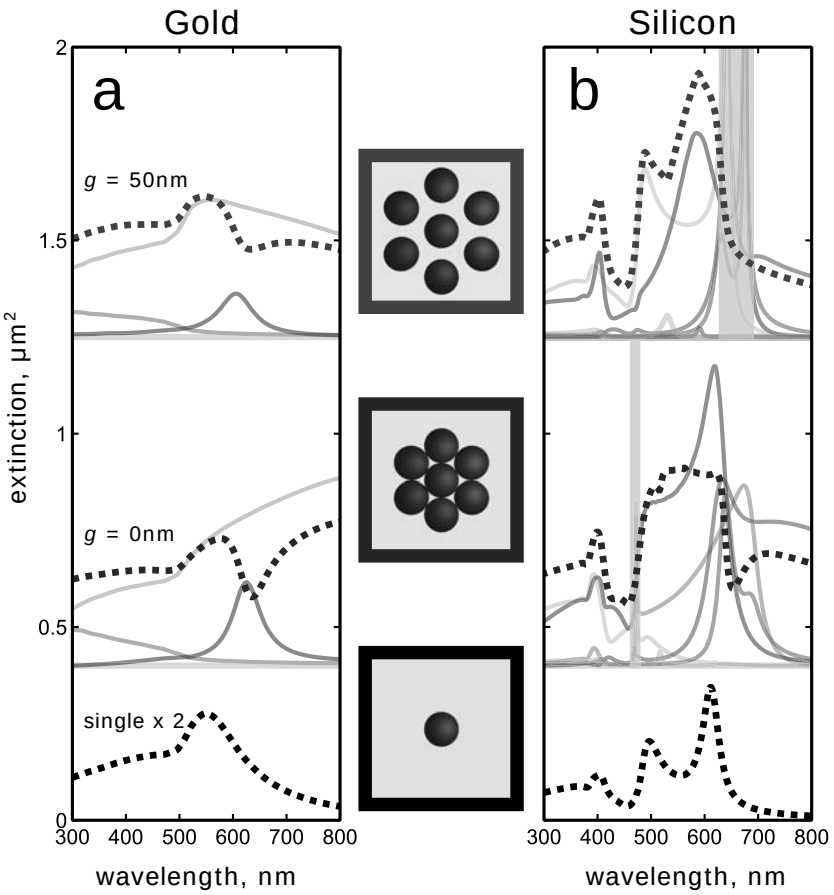

Fig. 10.3. (Dashed lines) Extinction spectra of (a) gold and (b) silicon heptamers, simulated using the dipole model Equation 10.8 and showing the role of eigenmode interference in producing Fano resonances. (Solid lines) Overlaid direct terms to extinction, as per Equation 10.20, for all three excited eigenmodes of the gold heptamers, and the six most dominant eigenmodes for the silicon heptamers. The gray regions correspond to wavelength bands near exceptional points. Both gold and silicon nanospheres are 150 nm in diameter.

to the projection of this eigenmode onto the complete incident field.

$$\sigma_{\mathrm{e}} = \frac{1}{I_0}\sqrt{\frac{\mu_0}{\epsilon_0}}\sum_{v}\ \mathrm{Re}\Big[a_v\big(\int_V \mathbf{E_0}^* \cdot \mathbf{J}_v\ \mathrm{d}\mathrm{r}^3\big)\Big] \tag{10.21}$$

In this approach, Fano resonances appear as negative extinction from an eigenmode [51], as per negative interference terms overpowering the positive direct terms. This decomposition ultimately contains the same interactions and

nonorthogonality of eigenmodes, however, it is still important to emphasize the role of modal overlap in producing Fano resonances: the eigenmodes themselves are the basis vectors that produce only positive extinction, and negative extinction only arises from the overlap between eigenmodes. The choice of deconstructing extinction using Equation 10.20 or 10.21, is effectively a question of whether or not to separate interference terms.

10.3.3 Eigenmodes of Nanoparticle Dimers

Up until now, the eigenmodes and eigenvalues we obtain have been calculated purely through numerics and we do not necessarily obtain information on the importance of geometric or design parameters. Here we will show a way to calculate the eigenmodes by subdividing the optical response of the complete structure into a set of constituent responses. In effect, what we will present resembles a so-called *hybridization* approach, but one that has been simplified and tailored for nanoparticle structures by using the electric and magnetic dipole model in Equations 10.8 and 10.14. Moreover, when considering relatively simple nanoparticle oligomer structures, it becomes possible to derive analytical expressions for the eigenmodes. This simplified approach of deriving the eigenmodes in terms of the constituent parts was introduced and presented for the case of a nanoparticle trimer [53]. Here, however, we will consider the more typical case of a nanoparticle dimer. There has been a recent surging interest in silicon nanoparticle dimers, which have been observed to exhibit behavior such as Fano resonances, directionality and magnetic near-field enhancement [57–59]. There is also an interest in hybrid dimers consisting both high-index dielectric nanoparticles *and* plasmonic nanoparticles, including predictions of antiferromagnetic behavior [60]. In any case, the complete solutions of the eigenmodes and eigenvalues in a symmetric dimer has previously been calculated analytically by Merchiers *et al* [47], although the scaling between electric and magnetic dipoles in Equation 10.14 was not accounted for. We will instead go further and demonstrate the simplified hybridization approach for the case of an *asymmetric* dimer. This will allow us to encompass some of these recent works that utilize asymmetry, but also the case of a particle on a substrate, where the substrate responds as a virtual image of the particle. However, to limit complexity, we restrict our analysis to diagonal tensor dipole polarizabilities with three primary axes (x, y and z axes), thereby neglecting both anisotropic and bianisotropic terms.

$$\bar{\alpha}_E^{(i)} = \begin{pmatrix} \alpha_{E|x}^{(i)} & & \\ & \alpha_{E|y}^{(i)} & \\ & & \alpha_{E|z}^{(i)} \end{pmatrix} \tag{10.22}$$

and similarly for $\bar{\alpha}_H$. We then use matrix notation to denote eigenmodes as vector concatenations of the associated dipole moments:

$$|v\rangle = \begin{pmatrix} \mathbf{p}_v^{(1)} \\ \mathbf{p}_v^{(2)} \\ c_0^{-1}\mathbf{m}_v^{(1)} \\ c_0^{-1}\mathbf{m}_v^{(2)} \end{pmatrix}, \quad \lambda|v\rangle = \begin{pmatrix} \mathbf{E}_{\mathbf{0}v}(\mathbf{r}_1) \\ \mathbf{E}_{\mathbf{0}v}(\mathbf{r}_2) \\ \sqrt{\frac{\mu_0}{\epsilon_0}}\mathbf{H}_{\mathbf{0}v}(\mathbf{r}_1) \\ \sqrt{\frac{\mu_0}{\epsilon_0}}\mathbf{H}_{\mathbf{0}v}(\mathbf{r}_2) \end{pmatrix} \tag{10.23}$$

The relative scaling of the electric and magnetic dipole moments, and of the electric and magnetic applied fields, is again used to define eigenmodes with consistent units and thereby ensure that the eigenvalues have units. Using the state notation in Equation 10.23, the eigenmode equation (Equation 10.14) can be compactly written in terms of both a polarizability operator $\hat{\boldsymbol{\alpha}}$ and a Green's function operator $\hat{\boldsymbol{\mathcal{G}}}$.

$$\lambda\,|v\rangle = \left(\hat{\boldsymbol{\alpha}}^{-1} - \hat{\boldsymbol{\mathcal{G}}}\right)|v\rangle \tag{10.24}$$

This allows us to find simplified matrix versions of the $\hat{\boldsymbol{\alpha}}$ and $\hat{\boldsymbol{\mathcal{G}}}$ operators for subsets of eigenmodes that transform according to a single irreducible representation of the dimer's symmetry point group. In particular, when considering the general case of an asymmetric dimer with achiral nanoparticles, we reduce the set of geometric symmetry operations to those of a C_{1h} point group. We can then define basis vectors of the dimer's optical response to be the eigenmodes of the $\hat{\boldsymbol{\mathcal{G}}}$ operator in the absence of electric to magnetic dipole coupling. These basis vectors are those shown in Fig. 10.4, which are named according to their irreducible representations in the C_{1h} point group, but with an additional subscript x, y, z to distinguish the orientation of each such basis vector and account for anisotropic nanoparticles as per Equation 10.22. Notably these basis vectors are more commonly associated with the eigenmodes of a symmetric dimer, but they are also practical for an asymmetric dimer because they still form a complete basis for its optical response. Moreover, because they remain eigenmodes of the Green's function operator in the absence of electric to magnetic coupling, we only need to consider coupling channels between basis vectors created by the $\hat{\boldsymbol{\alpha}}^{-1}$ operator, and the channels due to electric to magnetic coupling. In Fig. 10.4, we use the convention where a dashed line represents a coupling channel from the dissimilarity of nanoparticles in the $\hat{\boldsymbol{\alpha}}^{-1}$ polarizability operator and an unbroken line represents the bianisotropic coupling channels in the $\hat{\boldsymbol{\mathcal{G}}}$ Green's function operator. The magnitudes of these coupling channels can be determined from the polarizabilties of each nanoparticle, and from the dipole model in Equation 10.8.

$$\Delta\alpha^{-1} = \frac{1}{2}\left(\frac{1}{\alpha^{(1)}} - \frac{1}{\alpha^{(2)}}\right), \tag{10.25}$$

$$X_\uparrow = -X_\downarrow \equiv X = \frac{e^{ikR}}{4\pi\epsilon_0 R}\left(k^2 + \frac{ik}{R}\right) \tag{10.26}$$

We can also define the eigenvalues γ of the Green's function operator independently of the polarizability operator.

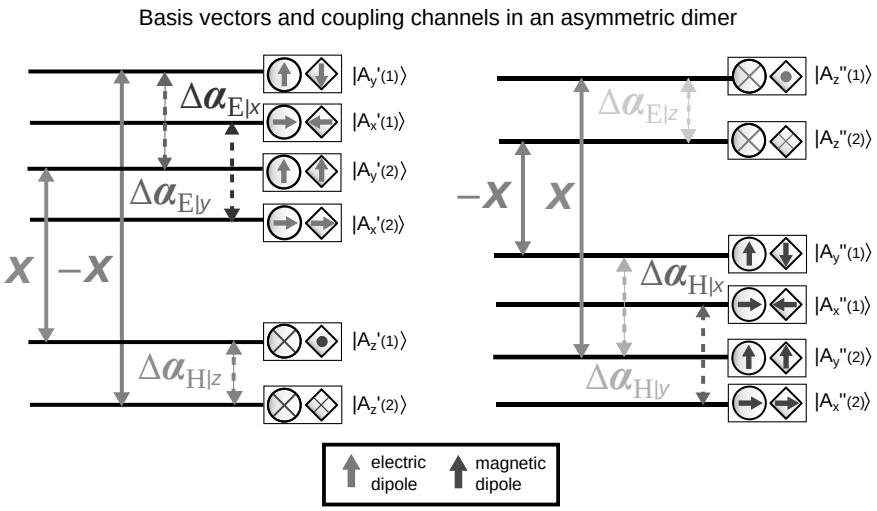

Fig. 10.4. Diagram showing the complete set of basis vectors, and the coupling channels between them, for the optical response of an asymmetric dimer. Individual nanoparticles are considered to exhibit both electric (red) and magnetic (blue) dipole moments.

$$\gamma_1 = \frac{e^{ikR}}{4\pi\epsilon_0 R}\Big(k^2 + \frac{ik}{R} - \frac{1}{R^2}\Big) \tag{10.27}$$

$$\gamma_2 = -\frac{e^{ikR}}{2\pi\epsilon_0 R}\Big(\frac{ik}{R} - \frac{1}{R^2}\Big) \tag{10.28}$$

where $R = |\mathbf{r}_1 - \mathbf{r}_2|$ is the distance between dipoles. Using this approach, the operator $\big(\hat{\boldsymbol{\alpha}}^{-1} - \hat{\boldsymbol{\mathcal{G}}}\big)$ can be written as a 2×2 matrix for each of the A'_x and A''_x basis vectors:

$$\hat{\boldsymbol{\alpha}}^{-1} - \hat{\boldsymbol{\mathcal{G}}} \;=\; \frac{1}{\epsilon_0}\begin{pmatrix} \langle\alpha^{-1}\rangle + \epsilon_0\gamma & \Delta\alpha^{-1} \\ \Delta\alpha^{-1} & \langle\alpha^{-1}\rangle - \epsilon_0\gamma \end{pmatrix} \tag{10.29}$$

where:

$$\Delta\alpha^{-1} = \frac{1}{2}\Big(\frac{1}{\alpha^{(1)}} - \frac{1}{\alpha^{(2)}}\Big)$$
$$\langle\alpha^{-1}\rangle = \frac{1}{2}\Big(\frac{1}{\alpha^{(1)}} + \frac{1}{\alpha^{(2)}}\Big)$$

The particular polarizability and component that α refers to has been left intentionally vague so we can reuse the notation; the particular values we use are listed in Tables 10.1 and 10.2.

For the remaining basis vectors of the complete dimer, the bianisotropic coupling channels require a 4×4 matrix in order to describe the $\hat{\boldsymbol{\alpha}}^{-1} - \hat{\boldsymbol{\mathcal{G}}}$ operator.

	$\lvert\Gamma^{(a)}\rangle$	$\lvert\Gamma^{(b)}\rangle$	$\alpha^{(1)}$	$\alpha^{(2)}$
A'_{x}	$\lvert\mathrm{A}'_{\mathrm{x}(1)}\rangle$	$\lvert\mathrm{A}'_{\mathrm{x}(2)}\rangle$	$\alpha^{(1)}_{E\lvert x}$	$\alpha^{(2)}_{E\lvert x}$
$\mathrm{A}''_{\mathrm{x}}$	$\lvert\mathrm{A}''_{\mathrm{x}(1)}\rangle$	$\lvert\mathrm{A}''_{\mathrm{x}(2)}\rangle$	$\alpha^{(1)}_{H\lvert x}$	$\alpha^{(2)}_{H\lvert x}$

Table 10.1. The combinations of basis vectors and polarizabilities that define pairs of eigenmodes for the A'_{x} and $\mathrm{A}''_{\mathrm{x}}$ responses, as described by Equation 10.32

.

$$\hat{\boldsymbol{\alpha}}^{-1} - \hat{\boldsymbol{\mathcal{G}}} = \frac{1}{\epsilon_0}\begin{pmatrix} \langle\alpha_E^{-1}\rangle + \epsilon_0\gamma_1 & \Delta\alpha_E^{-1} & & \epsilon_0 X \\ \Delta\alpha_E^{-1} & \langle\alpha_E^{-1}\rangle - \epsilon_0\gamma_1 & -\epsilon_0 X & \\ & \epsilon_0 X & \langle\alpha_H^{-1}\rangle + \epsilon_0\gamma_1 & \Delta\alpha_H^{-1} \\ -\epsilon_0 X & & \Delta\alpha_H^{-1} & \langle\alpha_H^{-1}\rangle - \epsilon_0\gamma_1 \end{pmatrix} \tag{10.30}$$

Here the indices of the polarizabilities are different for the A′ and A″ basis vectors as prescribed in Table 10.2. Given we now have equivalent matrix expressions for the independent subspaces of the $\hat{\boldsymbol{\alpha}}^{-1} - \hat{\boldsymbol{\mathcal{G}}}$ operator, shown in Equations 10.29 and 10.30, we can find the dimer's eigenmodes and eigenvalues such that they satisfy:

$$\lambda_v^{(i)}|v_i\rangle = (\hat{\boldsymbol{\alpha}}^{-1} - \hat{\boldsymbol{\mathcal{G}}})|v_i\rangle \tag{10.31}$$

In other words, the complete set of eigenmodes can be found from the eigendecompositions of 2×2 and 4×4 matrices. Moreover, for the case of the 2×2 matrices for A'_{x} and $\mathrm{A}''_{\mathrm{x}}$ reponse space, the eigenmodes and eigenvalues are of the form:

$$|v_\pm\rangle = \Big(\epsilon_0\gamma_2 \pm \delta_v\Big)|\Gamma^{(b)}\rangle - \Delta\alpha^{-1}|\Gamma^{(a)}\rangle \tag{10.32a}$$

$$\lambda_\pm = \frac{\langle\alpha^{-1}\rangle \mp \delta_v}{\epsilon_0} \tag{10.32b}$$

	A'	A''
α_E	$\alpha_{E\lvert y}$	$\alpha_{E\lvert z}$
α_H	$\alpha_{H\lvert z}$	$\alpha_{H\lvert y}$
X	X	$-X$

Table 10.2. The combinations of polarizability axes and coupling channel for Equations 10.35–10.38 that provide the eigenvalues and eigenmodes of the A′ and A″ irreducible representations according to Equation 10.39 and Equations 10.42–10.44

where the specific values to use for each polarizability α and the basis vectors $|\Gamma\rangle$ are written in Table 10.1, and we have also defined a function δ to explicitly quantify the difference between eigenmodes:

$$\delta_v = \frac{1}{\alpha^{(1)}\alpha^{(2)}}\sqrt{\left(\frac{\alpha^{(1)}-\alpha^{(2)}}{2}\right)^2 - \left(\alpha^{(1)}\alpha^{(2)}\epsilon_0\gamma\right)^2} \tag{10.33}$$

Equation 10.32 gives general expressions for the eigenmodes and eigenvalues of the A'_{x} and $\mathrm{A}''_{\mathrm{x}}$ reponse spaces. Notably, as per the discussion in Section 10.3.2, there is an *exceptional point* [56] occurring when $\delta = 0$; a degeneracy of eigenvalues combined with a linear dependency of the eigenmodes.

To find the remaining eigenvalues of the dimer, belonging to the $\hat{\boldsymbol{\alpha}}^{-1} - \hat{\boldsymbol{\mathcal{G}}}$ operator in Equation 10.30, we solve for the roots of the associated characteristic equation. The general form of the characteristic equation for both A' and A'' response spaces will be:

$$\lambda^4 + B\lambda^3 + C\lambda^2 + D\lambda + E = 0 \tag{10.34}$$

where each coefficient is given by Equations 10.35–10.38.

$$B = -\epsilon_0^{-1}\Big(\langle\alpha_E^{-1}\rangle + \langle\alpha_H^{-1}\rangle\Big) \tag{10.35}$$

$$C = \epsilon_0^{-2}\Big(\langle\alpha_E^{-1}\rangle\langle\alpha_H^{-1}\rangle + \frac{1}{\alpha_E^{(1)}\alpha_E^{(2)}} + \frac{1}{\alpha_H^{(1)}\alpha_H^{(2)}} + 2\epsilon_0^2\big(X^2-\gamma_1^2\big)\Big) \tag{10.36}$$

$$D = \epsilon_0^{-3}\Big(\langle\alpha_E^{-1}\rangle\Big[\epsilon_0^2\gamma_1^2 - \frac{1}{\alpha_H^{(1)}\alpha_H^{(2)}}\Big] + \langle\alpha_E^{-1}\rangle\Big[\epsilon_0^2\gamma_1^2 - \frac{1}{\alpha_E^{(1)}\alpha_E^{(2)}}\Big] - \epsilon_0^2X^2\Big[\langle\alpha_E^{-1}\rangle + \langle\alpha_H^{-1}\rangle\Big]\Big) \tag{10.37}$$

$$E = \epsilon_0^{-4}\Big(\frac{1}{\alpha_E^{(1)}\alpha_E^{(2)}\alpha_H^{(1)}\alpha_H^{(2)}} + \epsilon_0^2X^2\Big[\frac{1}{\alpha_E^{(1)}\alpha_H^{(2)}} + \frac{1}{\alpha_H^{(1)}\alpha_E^{(2)}}\Big] - \epsilon_0^2\gamma_1^2\Big[\frac{1}{\alpha_E^{(1)}\alpha_E^{(2)}} + \frac{1}{\alpha_H^{(1)}\alpha_H^{(2)}}\Big] + \epsilon_0^4(X^2-\gamma_1^2)^2\Big) \tag{10.38}$$

The roots of quartic equations like Equation 10.34 are known for general coefficients. Indeed, we write the resulting eigenvalues using four different combinations of plus and minus signs, $\pm_{(1)}$ and $\pm_{(2)}$:

$$\lambda \;=\; -\frac{1}{4}B \;\pm_{(1)}\; \frac{1}{2}\sqrt{\frac{1}{4}B^2 - C + h} \;\pm_{(2)}\; \frac{1}{2}\sqrt{\frac{1}{2}B^2 - C - h \;\pm_{(1)}\; \frac{-\frac{1}{4}B^3 + BC - 2D}{\sqrt{\frac{1}{4}B^2 - C + h}}} \tag{10.39a}$$

$$\lambda \;\to\; -\frac{1}{4}B \;\pm_{(2)}\; \frac{1}{2}\sqrt{\frac{3}{4}B^2 - 2C \;\pm_{(1)}\; 2\sqrt{h^2 - 4E}}, \quad \text{when} \quad \frac{1}{4}B^2 - C + h = 0 \tag{10.39b}$$

where :

$$h = \frac{1}{3}\left(C + q\left[\frac{p + \sqrt{p^2 - 4q^3}}{2}\right]^{-1/3} + \left[\frac{p + \sqrt{p^2 - 4q^3}}{2}\right]^{1/3}\right)$$
$$p = 2C^3 - 9BCD + 27D^2 + 27B^2E - 72CE$$
$$q = C^2 - 3BD + 12E$$

Using these eigenvalues we can now find the dipole moment profiles of the eigenmodes themselves. We begin by writing an eigenmode as a linear combination of the associated A′ and A″ basis vectors,

$$|v_i\rangle = \begin{cases} a_i|\mathrm{A}'_{(\mathrm{y2})}\rangle + b_i|\mathrm{A}'_{(\mathrm{y1})}\rangle + c_i|\mathrm{A}'_{(\mathrm{z2})}\rangle + d_i|\mathrm{A}'_{(\mathrm{z1})}\rangle & (A') \\ a_i|\mathrm{A}''_{(\mathrm{y2})}\rangle + b_i|\mathrm{A}''_{(\mathrm{y1})}\rangle + c_i|\mathrm{A}''_{(\mathrm{z2})}\rangle + d_i|\mathrm{A}''_{(\mathrm{z1})}\rangle & (A'') \end{cases} \tag{10.40}$$

We can then write down the relationships between the coefficients of these A′ and A″ basis vectors using the coupling channels depicted by Figure 10.4 and expressed in Equation 10.30.

$$Xd_i = \left(\lambda_i - \tfrac{1}{\epsilon_0}\langle\alpha_E^{-1}\rangle + \gamma_1\right)a_i - \tfrac{1}{\epsilon_0}\Delta\alpha_E^{-1}b_i \tag{10.41a}$$
$$-Xc_i = \left(\lambda_i - \tfrac{1}{\epsilon_0}\langle\alpha_E^{-1}\rangle - \gamma_1\right)b_i - \tfrac{1}{\epsilon_0}\Delta\alpha_E^{-1}a_i \tag{10.41b}$$
$$Xb_i = \left(\lambda_i - \tfrac{1}{\epsilon_0}\langle\alpha_H^{-1}\rangle - \gamma_1\right)c_i - \tfrac{1}{\epsilon_0}\Delta\alpha_H^{-1}d_i \tag{10.41c}$$
$$-Xa_i = \left(\lambda_i - \tfrac{1}{\epsilon_0}\langle\alpha_H^{-1}\rangle + \gamma_1\right)d_i - \tfrac{1}{\epsilon_0}\Delta\alpha_H^{-1}c_i \tag{10.41d}$$

By substituting between these equations, we can obtain the following expressions for the ratios between coefficients:

$$\frac{a_i}{b_i} = \frac{-(\lambda_i+\gamma_1)\frac{1}{\epsilon_0}\langle\alpha_E^{-1}\rangle - (\lambda_i-\gamma_1)\frac{1}{\epsilon_0}\langle\alpha_H^{-1}\rangle + (\lambda_i^2-\gamma_1^2) + \frac{1}{2\epsilon_0^2}\left(\frac{1}{\alpha_E^{(1)}\alpha_H^{(2)}} + \frac{1}{\alpha_E^{(2)}\alpha_H^{(1)}}\right) + X^2}{(\lambda_i+\gamma_1)\frac{1}{\epsilon_0}(\Delta\alpha_E^{-1} - \Delta\alpha_H^{-1}) + \frac{1}{2\epsilon_0^2}\left(\frac{1}{\alpha_E^{(2)}\alpha_H^{(1)}} - \frac{1}{\alpha_E^{(1)}\alpha_H^{(2)}}\right)} \tag{10.42}$$

$$\frac{c_i}{d_i} = \frac{(\lambda_i-\gamma_1)\frac{1}{\epsilon_0}\langle\alpha_E^{-1}\rangle + (\lambda_i+\gamma_1)\frac{1}{\epsilon_0}\langle\alpha_H^{-1}\rangle - (\lambda_i^2-\gamma_1^2) - \frac{1}{2\epsilon_0^2}\left(\frac{1}{\alpha_E^{(1)}\alpha_H^{(2)}} + \frac{1}{\alpha_E^{(2)}\alpha_H^{(1)}}\right) - X^2}{(\lambda_i+\gamma_1)\frac{1}{\epsilon_0}(\Delta\alpha_E^{-1} - \Delta\alpha_H^{-1}) + \frac{1}{2\epsilon_0^2}\left(\frac{1}{\alpha_E^{(2)}\alpha_H^{(1)}} - \frac{1}{\alpha_E^{(1)}\alpha_H^{(2)}}\right)} \tag{10.43}$$

$$\begin{aligned}\frac{d_i}{b_i} = {} & \frac{1}{X\Big((\lambda_i+\gamma_1)\frac{1}{\epsilon_0}(\Delta\alpha_E^{-1} - \Delta\alpha_H^{-1}) + \frac{1}{2\epsilon_0^2}\left(\frac{1}{\alpha_E^{(2)}\alpha_H^{(1)}} - \frac{1}{\alpha_E^{(1)}\alpha_H^{(2)}}\right)\Big)} \cdot \\ & \left[\frac{1}{\epsilon_0}\Big(\big(\lambda_i^2-\gamma_1^2\big)\langle\alpha_H^{-1}\rangle + X^2\langle\alpha_E^{-1}\rangle\Big) - \big(\lambda_i+\gamma_1\big)\big(\lambda_i^2-\gamma_1^2+X^2\big)\right. \\ & \left. + \Big(\frac{1}{\epsilon_0}\langle\alpha_H^{-1}\rangle - (\lambda_i+\gamma_1)\Big)\Big(\frac{1}{\alpha_E^{(1)}\alpha_E^{(2)}\epsilon_0^2} - \frac{2}{\epsilon_0}\langle\alpha_E^{-1}\rangle\lambda_i\Big)\right]\end{aligned} \tag{10.44}$$

These three ratios are sufficient to produce expressions for each eigenmode when normalized to b_i, a dependence that is removed by simply normalizing each eigenmode. In Figure 10.5a, we demonstrate that this analytical expression for the eigenmodes is able to accurately predict the optical extinction of an asymmetric dimer made from silicon nanospheres. The dimer we consider also doubles as an example of how electric to magnetic coupling can be utilized, in this case for directional scattering. Moreover, referring to Figure 10.1, we see that the magnetic dipole resonance of a 150 nm silicon sphere roughly coincides with the electric resonance of a 200 nm silicon sphere. If we, therefore, arrange two such spheres as a dimer, we can utilize the coupling to mix electric and magnetic resonances of the single particles into collective modes. The 150 nm silicon sphere's magnetic dipole resonance is stronger than the 200 nm silicon sphere's electric dipole resonance. So, with normal incidence plane wave excitation and magnetic field polarization perpendicular to the axis of the dimer, we couple the single particle magnetic resonance with the electric dipoles parallel to propagation direction (*c.f.* Figure 10.4), allowing for collective resonances that are averaged between the magnetic and electric resonances. The coupling can then be controlled by simply adjusting the gap between the two silicon nanospheres, allowing us to equalize the total electric and magnetic dipole moments from this collective system to approach the conditions for Huygen's sources [27] or weak duality symmetry [61, 62]. Indeed, as seen in Figure 10.5b, this approach leads to strong directional scattering, which is a result of an equality of the total electric and magnetic dipole moments in this system seen through Figure 10.5c. Notably, this approach *maximizes* the scattering, as distinct from recent realizations of silicon nanosphere dimers that produce directional scattering by utilizing Fano resonances, which *minimize* scattering [57].

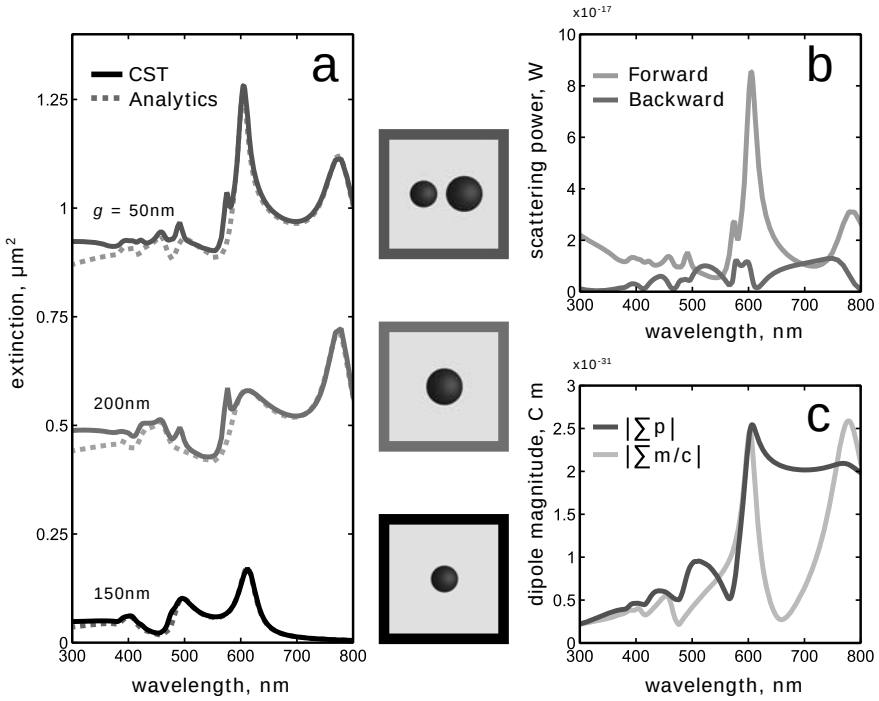

Fig. 10.5. (a) Calculated extinction spectra for a 150 nm and a 200 nm diameter silicon nanosphere, and the combined dimer when separated by $g = 50$ nm, showing good agreement between CST and the analytical result for eigenmodes and eigenvalues derived in this section. (b) The forward and backward scattered power in $\pi/6$ solid angles of a plane wave with unit amplitude (1 V/m), and (c) the associated equality of electric and magnetic dipoles in the dimer.

To understand our dimer system further, we provide analysis of its behavior from the perspective of the collective eigenmodes. Indeed, in Figure 10.6, we see how the previous description of coupling between magnetic dipoles and electric dipoles parallel to the propagation direction can be related to three particular eigenmodes. Figure 10.6a shows the individual eigenmode contributions to extinction, and that the directional scattering at 600 nm wavelength can be dominantly attributed to the three eigenmodes (i-iii), whose profiles are depicted in Figure 10.6b. The first two eigenmodes (i and ii) are dominated by the pure electric and magnetic dipole of the 200 nm and 150 nm nanoparticles, respectively. A third eigenmode (iii) then also contributes to the magnetic dipole of the 150 nm nanoparticle, while being significantly dependent on electric dipoles aligned parallel to the propagation direction, and thereby providing the extra degree of freedom to balance the final magnitudes of the electric and magnetic dipoles in the 200 nm and 150 nm nanoparticles. The combination of these three eigenmodes then describes the directional scat-

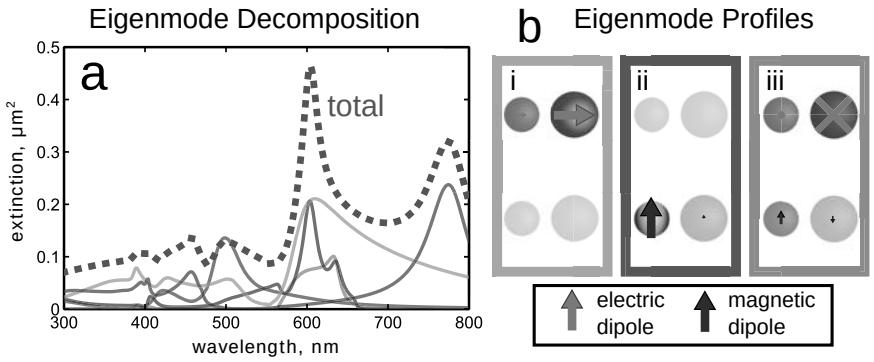

Fig. 10.6. (a) Eigenmode decomposition of the extinction from the silicon nanosphere dimer in Figure 10.5a. (b) The electric and magnetic dipole moments of the three most dominant eigenmodes that contribute towards the extinction peak at 600 nm.

tering we observed in Figure 10.5b, in a way that is related to the collective resonances of the nanoparticle dimer. This thereby demonstrates one avenue by which eigenmodes can be used to gain insight into the collective optical resonances and operation of dielectric nanoparticle oligomers.

10.3.4 Dimensionless Eigenvalues

The eigenmodes and the eigenvalues we have presented up until now have been to understand a polarizability relationship between either dipoles or currents and the driving field. However, in some situations, it may also be informative to know the eigenmodes of a geometry where there is no driving field, such as in the transient response to excitation by a pulse of light. These eigenmodes of the undriven system, having current distributions $\boldsymbol{\mathcal{J}}_v$, represent the underlying stable currents or dipole moments of a given structure; they are the stable oscillations that persist in the given structure when the driving field is removed. Notably, the associated eigenvalues Λ_v of this situation are then not polarizabilities, but rather dimensionless values for the self-feedback strength of the given current or dipole distribution.

$$\Lambda_v \boldsymbol{\mathcal{J}}_v(\mathbf{r}) = \big(\bar{\epsilon}(\mathbf{r}) - \epsilon_0\big)\frac{k^2}{\epsilon_0}\int_V \bar{G}_0(\mathbf{r},\mathbf{r}')\boldsymbol{\mathcal{J}}_v(\mathbf{r}')\,\mathrm{d}^3x' \tag{10.45}$$

Comparing this expression to Equation 10.10, we can see that there is no distinction between eigenmodes with or without a driving field when the given structure is made up of a homogeneous isotropic material. It is only when we introduce additional materials into our scattering system that the stable resonances are changed by the presence of a driving field. However, if we consider the analogous situation for the dipole model in Equation 10.5, the

eigenmodes of Equations 10.10 and 10.45 become distinct as soon as there is more than one single isotropic polarizability for describing all dipoles. As a consequence, there will generally be a distinction between the two types of eigenmodes whenever a dipole system consists of both electric and magnetic dipoles. Moreover, we can consider eigenmodes $\{\boldsymbol{\mathcal{P}}_v, \boldsymbol{\mathcal{M}}_v\}$ of the electric and magnetic dipole model in Equation 10.8 when there is no driving field.

$$\Lambda_v \boldsymbol{\mathcal{P}}_v^{(i)} = \alpha_E^{(i)} k^2 \left(\sum_{j \neq i} \bar{G}_0(\mathbf{r}_i, \mathbf{r}_j) \cdot \boldsymbol{\mathcal{P}}_v^{(j)} - \frac{1}{c_0} \nabla \times \bar{G}_0(\mathbf{r}_i, \mathbf{r}_j) \cdot \boldsymbol{\mathcal{M}}_v^{(j)} \right) \quad (10.46a)$$

$$\Lambda_v \boldsymbol{\mathcal{M}}_v^{(i)} = \alpha_H^{(i)} k^2 \left(\sum_{j \neq i} \bar{G}_0(\mathbf{r}_i, \mathbf{r}_j) \cdot \boldsymbol{\mathcal{M}}_v^{(j)} + c_0 \nabla \times \bar{G}_0(\mathbf{r}_i, \mathbf{r}_j) \cdot \boldsymbol{\mathcal{P}}_v^{(j)} \right) \quad (10.46b)$$

This expression will produce different eigenmodes to that of Equation 10.14, but it serves to provide different insights into the given scattering system. Notably, we do not need to scale the electric and magnetic dipoles to have correct units for the eigenvalue: it now remains unitless for any scaling between electric and magnetic dipoles.

10.4 Observation of Fano Resonances in Nanoparticle Oligomers

The study of Fano resonances in plasmonic nanoparticle structures has a long history, whereas the theoretical predictions [21, 63] and experimental demonstrations [14, 25, 26, 53, 57] of Fano resonances in all-dielectric nanoparticle oligomers have been reported only recently. In comparison to the oligomers composed of plasmonic nanoparticles, all-dielectric oligomer structures support both strong electric and magnetic resonances in the individual constituent elements and open up a whole new dimension for mutual inter-element coupling and, consequently, for the formation of collective modes. Indeed, it was recently predicted in theory [21, 63] that light scattering by silicon oligomers should exhibit well-pronounced Fano resonances originating from the predominant excitation of optically-induced magnetic dipole modes in the individual elements of the oligomer structure.

The Fano resonance is traditionally recognized as arising from the interference of broad and narrow spectral lines, yet the concept can be also extended to encompass the situation of interference between several electric and/or magnetic modes of comparable spectral width [21]. Importantly, the resulting asymmetric line-shape of the Fano resonance is still clearly observed in both theory and experiment since the destructive and constructive interference take place in a narrow spectral range exhibiting strongly resonant response. The existence of such Fano resonances in silicon oligomers might offer a range of novel possibilities for applications, owing to their higher resistance to heat as compared to optical metal nanostructures and to the possibility of free carrier

generation in the material. In this regard, Figure 10.7 presents the experimental results for the observation of Fano resonances in heptamer oligomers composed of Si nanodisks. In particular, Fig. 10.7a shows top view SEM images of several heptamer structures arranged in two-dimensional arrays with a lattice constant of 2840 nm. This value has been chosen in order to ensure that the separation between neighboring structures is large enough for dominant coupling to remain within each oligomer structure, while the in-plane density of oligomer structures is still sufficiently high to create pronounced resonances in the far-field spectra. The measurement results of linear-optical transmittance spectra from four, silicon nanodisk heptamer arrays, with varying central nanodisk diameter and unpolarized incident light, are presented in Figure 10.7b. The experimental and theoretical extinction spectra show

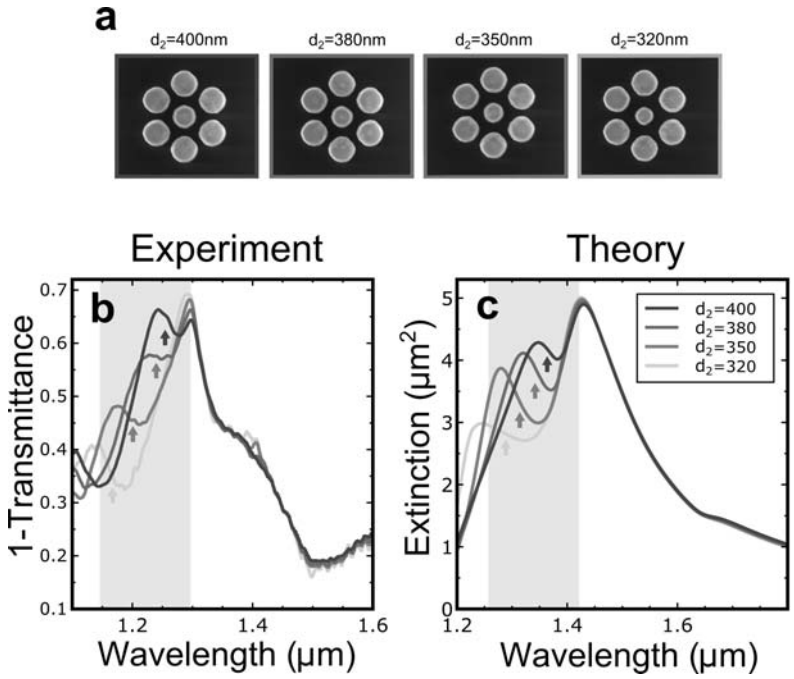

Fig. 10.7. Experimental observation of Fano resonances in Si oligomers. (a) Scanning electron micrographs of heptamer oligomers. (b,c) Extinction spectra for a variety of silicon nanodisk structures featuring a systematic variation of the central nanodisk diameter. Shown are (b) experimentally measured results for arrayed structures with unpolarized incident light, and (c) theoretically calculated results for single heptamers for arbitrarily polarized light. A Fano resonance is created in the heptamers (see gray-shaded region and colored arrows), and it moves across the spectrum as the diameter of the central particle is varied [25].

a good qualitative agreement. In both sets of results two distinct extinction peaks for each spectrum are observed. The peak at longer wavelengths corresponds to the magnetic resonance of the collective structure. The second peak, which is observed at shorter wavelengths, is associated with the magnetic resonance of the central particle. By analyzing the major collective modes of the oligomer structures corresponding with its dominant resonances, numerical calculations [25] further unveil the main mechanism of eigenmode interference realized in the heptamer structures. This confirms that the observed Fano resonances indeed originate from interference between the optically-induced magnetic resonances of the central particles and those of the collective structures.

Later, Filonov *et al.* [64] demonstrated the existence of Fano resonances in all-dielectric oligomer structures in a series of microwave experiments. They confirmed this result by both far- and near-field measurements, including the studies of the forward scattering and phase distribution across the structure. The resonant suppression of the scattering was observed to be accompanied by a π phase jump at the central particle, and this was confirmed by the modal analysis based on the coupled-dipole approximation, which allows one to clearly identify the particular supermodes contributing to the resonant interference phenomena. In addition, the authors observed a unique type of Fano resonance in hexamer oligomers without a central particle; this type of Fano resonance originates from the interference of electric-type supermodes, and it exhibits an asymmetric profile due to the presence of both constructive and destructive interference phenomena.

Because dielectric nanoparticles enable a different coupling mechanism between electric and magnetic resonances, Fano resonances can be clearly observed for smaller number of particles such as trimers [53] and quadrumers [26]. In particular, the magnetic field polarized along a symmetric quadrumer's principal axis can produce a resonant circulation of field that can couple to the inherent magnetic response of the individual nanoparticles. The interference between magnetic responses can then be tailored to produce distinctive and sharp magnetic Fano resonances [26]. This form of optically induced magnetic–magnetic coupling and interference is a unique characteristic of properly designed dielectric nanoclusters. To verify the theoretical predictions experimentally, Hopkins *et al.* [26] studied scattering properties of $MgOTiO_2$ ceramic spheres characterized by a dielectric constant of 16 measured at 9–12 GHz. These ceramic spheres in the microwave range therefore have very similar properties to silicon nanospheres in the optical range, and they were employed as a useful macroscopic platform on which to prototype silicon nanostructures. The MgO-TiO_2 quadrumer consists of four dielectric spheres with diameter 15 mm, and the size of the gap between the particles is 5 mm. The experimentally measured, and numerically calculated, total scattering of the quadrumer structure is shown in Figure 10.8. It can clearly be seen that a magnetic Fano resonance is produced at 5.4 GHz in both simulation and experiment. This was the first example of a magnetic–magnetic Fano

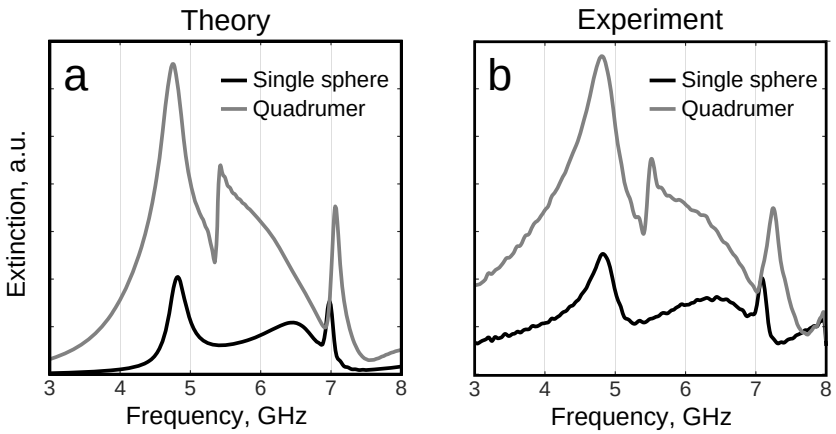

Fig. 10.8. Comparison between theoretical and experimental results for quadrumer oligomers. (a) Numerical simulation results and (b) experimental measurements of extinction for a quadrumer made of four $MgOTiO_2$ ceramic spheres. Also shown is the extinction from a single MgO-TiO_2 sphere for reference. In both simulation and experiment the existence of a sharp Fano resonance occurring at 5.4 GHz is detected [26].

resonance in a single symmetric metamolecule. Notably, this Fano resonance occurs in a spectral range where the single particle is not at resonance, which demonstrates its collective nature. Indeed, it appears near the intersection of the single particle's electric and magnetic scattering contributions, reflecting that the overlap of eigenmodes is dependent on both electric and magnetic dipole polarizabilities. The role of individual electric and magnetic dipoles has also been considered relating to Fano resonances arising from the interaction between broad and narrow modes in dimers composed of two different silicon nanospheres [57]. The silicon nanosphere dimer exhibits a strong internal magnetic response, with an electric enhancement in the gap, providing an excellent structure to support magnetic-based Fano scattering. The interactions between magnetic and electric dipoles can then suppress backward scattering and enhance forward scattering at Fano wavelengths. This directional scattering is much more prominent than that from a single silicon sphere and shows promising applications in areas such as directional nanoantennas or optical switching, opening up future avenues for developing all-dielectric nanophotonic devices.

10.5 Concluding Remarks

The study of resonant dielectric and semiconductor nanoparticle structures has become a new research direction in modern optics and nanophotonics. Due to their unique optically-induced Mie-type electric and magnetic resonances,

such high-index dielectric photonic structures are expected to complement or substitute some of the plasmonic components in a range of potential applications. The unique low-loss resonant behavior makes it possible to reproduce many subwavelength resonant effects demonstrated in nanophotonics without much energy dissipation into heat. In addition, the co-existence of strong electric and magnetic resonances, their interference and resonant enhancement of the magnetic response in dielectric nanoparticles bring new physics and entirely novel functionalities to simple nanoparticle geometries. This is a direction that has not been much explored, especially in the nonlinear regime.

References

1. A. B. Evlyukhin, C. Reinhardt, A. Seidel, B. S. Luk'yanchuk, and B. N. Chichkov, "Optical response features of Si-nanoparticle arrays," *Phys. Rev. B*, vol. 82, p. 045404, 2010.
2. A. E. Krasnok, A. E. Miroshnichenko, P. A. Belov, and Y. S. Kivshar, "Huygens optical elements and Yagi-Uda nanoantennas based on dielectric nanoparticles," *JETP. Lett.*, vol. 94, no. 8, p. 593, 2011.
3. A. García-Etxarri, R. Gómez-Medina, L. S. Froufe-Pérez, C. López, L. Chantada, F. Scheffold, J. Aizpurua, M. Nieto-Vesperinas, and J. J. Sáenz, "Strong magnetic response of submicron silicon particles in the infrared," *Opt. Express*, vol. 19, pp. 4815–4826, 2011.
4. M. Kerker, "Invisible bodies," *J. Opt. Soc. Am.*, vol. 65, pp. 376–379, 1975.
5. M. Nieto-Vesperinas, R. Gomez-Medina, and J. J. Saenz, "Angle-suppressed scattering and optical forces on submicrometer dielectric particles," *J. Opt. Soc. Am. A*, vol. 28, no. 1, pp. 54–60, 2011.
6. B. Rolly, B. Stout, and N. Bonod, "Boosting the directivity of optical antennas with magnetic and electric dipolar resonant particles," *Opt. Express*, vol. 20, no. 18, pp. 20376–20386, 2012.
7. J. M. Geffrin, B. Garca-Cámara, P. A. R. Gómez-Medina, L. S. Froufe-Pérez, C. Eyraud, A. Litman, R. Vaillon, F. Gonzáleź, M. Nieto-Vesperinas, J. J. Sáenz, and F. Moreno, "Magnetic and electric coherence in forward- and back-scattered electromagnetic waves by a single dielectric subwavelength sphere," *Nat. Commun.*, vol. 3, p. 1171, 2012.
8. A. I. Kuznetsov, A. E. Miroshnichenko, Y. H. Fu, J. B. Zhang, and B. Luk'yanchuk, "Magnetic light," *Sci. Rep.*, vol. 2, p. 492, 2012.
9. A. B. Evlyukhin, S. M. Novikov, U. Zywietz, R. L. Eriksen, C. Reinhardt, S. I. Bozhevolnyi, and B. N. Chichkov, "Demonstration of magnetic dipole resonances of dielectric nanospheres in the visible region," *Nano Lett.*, vol. 12, pp. 3749–3755, 2012.
10. W. Liu, A. E. Miroshnichenko, D. N. Neshev, and Y. S. Kivshar, "Broadband unidirectional scattering by magneto-electric core-shell nanoparticles," *ACS Nano*, vol. 6, no. 6, p. 5489, 2012.
11. Y. H. Fu, A. I. Kuznetsov, A. E. Miroshnichenko, Y. F. Yu, and B. Luk'yanchuk, "Directional visible light scattering by silicon nanoparticles," *Nat. Commun.*, vol. 4, p. 1527, 2013.

12. W. Liu, A. E. Miroshnichenko, and Y. S. Kivshar, "Control of light scattering by nanoparticles with optically-induced magnetic responses," *Chin. Phys. B*, vol. 23, no. 23, p. 047806, 2014.
13. A. E. Krasnok, A. E. Miroshnichenko, P. A. Belov, and Y. S. Kivshar, "All-dielectric optical nanoantennas," *Opt. Express*, vol. 20, no. 18, p. 20599, 2012.
14. D. S. Filonov, A. E. Krasnok, A. P. Slobozhanyuk, P. V. Kapitanova, E. A. Nenasheva, Y. S. Kivshar, and P. A. Belov, "Experimental verification of the concept of all-dielectric nanoantennas," *Appl. Phys. Lett.*, vol. 100, p. 201113, 2012.
15. A. Krasnok, C. Simovski, P. Belov, and Y. S. Kivshar, "Superdirective dielectric nanoantenna," *Nanoscale*, vol. 6, pp. 7354–7361, 2014.
16. A. E. Miroshnichenko, S. Flach, and Y. S. Kivshar, "Fano resonances in nanoscale structures," *Rev. Mod. Phys.*, vol. 82, pp. 2257–2298, 2010.
17. B. Luk'yanchuk, N. I. Zheludev, S. A. Maier, N. J. Halas, P. Nordlander, H. Giessen, and C. T. Chong, "The Fano resonance in plasmonic nanostructures and metamaterials," *Nature Materials*, vol. 9, pp. 707–715, 2010.
18. Y. S. Joe, A. M. Satanin, and C. S. Kim, "Classical analogy of Fano resonances," *Phys. Scr.*, vol. 74, pp. 259–266, 2006.
19. B. Gallinet and O. J. F. Martin, "Ab initio theory of Fano resonances in plasmonic nanostructures and metamaterials," *Phys. Rev. B*, vol. 83, p. 235427, 2011.
20. H. H. Sheinfux, I. Kaminer, Y. Plotnik, G. Bartal, and M. Segev, "Subwavelength multilayer dielectrics: Ultrasensitive transmission and breakdown of effective-medium theory," *Phys. Rev. Lett.*, vol. 113, p. 243901, 2014.
21. B. Hopkins, A. N. Poddubny, A. E. Miroshnichenko, and Y. S. Kivshar, "Revisiting the physics of Fano resonances for nanoparticle oligomers," *Phys. Rev. A*, vol. 88, p. 053819, 2013.
22. A. I. Kuznetsov, "Light manipulation by resonant dielectric nanostructures and metasurfaces," in *Proc. SPIE 9544, Metamaterials, Metadevices, and Metasystems 2015*, p. 95442A, 2015.
23. I. Staude, A. E. Miroshnichenko, M. Decker, N. T. Fofang, S. Liu, E. Gonzales, J. Dominguez, T. S. Luk, D. N. Neshev, I. Brener, and Y. Kivshar, "Tailoring directional scattering through magnetic and electric resonances in subwavelength silicon nanodisks," *ACS Nano*, vol. 7, no. 9, pp. 7824–7832, 2013.
24. B. S. Luk'yanchuk, N. V. Voshchinnikov, R. Paniagua-Domínguez, and A. I. Kuznetsov, "Optimum forward light scattering by spherical and spheroidal dielectric nanoparticles with high refractive index," *ACS Photon.*, vol. 2, no. 7, pp. 993–999, 2015.
25. K. E. Chong, B. Hopkins, I. Staude, A. E. Miroshnichenko, J. Dominguez, M. Decker, D. N. Neshev, I. Brener, and Y. S. Kivshar, "Observation of Fano Resonances in All-Dielectric Nanoparticle Oligomers," *Small*, vol. 10, no. 10, pp. 1985–1990, 2014.
26. B. Hopkins, D. S. Filonov, A. E. Miroshnichenko, F. Monticone, A. Alù, and Y. S. Kivshar, "Interplay of magnetic responses in all-dielectric oligomers to realize magnetic Fano resonances," *ACS Photon.*, vol. 2, pp. 724–729, 2015.
27. C. Pfeiffer and A. Grbic, "Metamaterial huygens' surfaces: Tailoring wave fronts with reflectionless sheets," *Phys. Rev. Lett.*, vol. 110, p. 197401, May 2013.
28. M. Decker, I. Staude, M. Falkner, J. Dominguez, D. N. Neshev, I. Brener, T. Pertsch, and Y. S. Kivshar, "High-Efficiency Dielectric Huygens' Surfaces," *Adv. Opt. Mater.*, vol. 3, pp. 813–820, 2015.

29. K. E. Chong, I. Staude, A. James, J. Dominguez, S. Liu, S. Campione, G. S. Subramania, T. S. Luk, M. Decker, I. B. Dragomir N. Neshev and, and Y. S. Kivshar, "Polarization-independent silicon metadevices for efficient optical wavefront control," *Nano Lett.*, vol. 15, no. 8, pp. 5369–5374, 2015.
30. A. Arbabi, Y. Horie, M. Bagheri, and A. Faraon, "Dielectric metasurfaces for complete control of phase and polarization with subwavelength spatial resolution and high transmission," *Nat. Mat.*, vol. 10, pp. 937–944, 2015.
31. A. D. Yaghjian, "Electric Dyadic Green's Functions in the Source Region," *Proc. IEEE*, vol. 68, no. 2, pp. 248–263, 1980.
32. D. A. Powell, "Resonant dynamics of arbitrarily shaped meta-atoms," *Phys. Rev. B*, vol. 90, p. 075108, 2014.
33. M. Hentschel, M. Saliba, R. Vogelgesang, H. Giessen, A. P. Alivisatos, and N. Liu, "Transition from isolated to collective modes in plasmonic oligomers," *Nano Lett.*, vol. 10, pp. 2721–2726, 2010.
34. B. Hopkins, W. Liu, A. E. Miroshnichenko, and Y. S. Kivshar, "Optically isotropic responses induced by discrete rotational symmetry of nanoparticle clusters," *Nanoscale*, vol. 5, pp. 6395–6403, 2013.
35. M. Rahmani, E. Yoxall, B. Hopkins, Y. Sonnefraud, Y. Kivshar, M. Hong, C. Phillips, S. A. Maier, and A. E. Miroshnichenko, "Plasmonic nanoclusters with rotational symmetry: Polarization-invariant far-field response vs changing near-field distribution," *ACS Nano*, vol. 7, pp. 11138–11146, 2013.
36. G. W. Mulholland, C. F. Bohren, and K. A. Fuller, "Light scattering by agglomerates: Coupled electric and magnetic dipole method," *Langmuir*, vol. 10, no. 8, p. 2533, 1994.
37. B. T. Draine and P. J. Flatau, "Discrete-dipole approximation for scattering calculations," *J. Opt. Soc. Am. A*, vol. 11, pp. 1491–1499, Apr 1994.
38. G. Mie, "Beitrage zur optik truber medien," *Ann. Phys.*, vol. 25, pp. 377–445, 1908.
39. C. F. Bohren and D. R. Huffman, *Absorption and scattering of light by small particles*. New York: Wiley, 1983.
40. J. Chen, J. Ng, Z. Lin, and C. T. Chan, "Optical pulling force," *Nat. Photon.*, vol. 5, pp. 531–534, 2011.
41. P. Grahn, A. Shevchenko, and M. Kaivola, "Electromagnetic multipole theory for optical nanomaterials," *New J. Phys.*, vol. 14, p. 093033, 2012.
42. A. E. Miroshnichenko, A. B. Evlyukhin, Y. F. Yu, R. M. Bakker, A. Chipouline, A. I. Kuznetsov, B. Luk'yanchuk, B. N. Chichkov, and Y. S. Kivshar, "Nonradiating anapole modes in dielectric nanoparticles," *Nat. Commun.*, vol. 6, p. 8069, 2015.
43. F. B. Arango and A. F. Koenderink, "Polarizability tensor retrieval for magnetic and plasmonic antenna design," *New J. Phys.*, vol. 15, p. 073023, 2013.
44. L. D. Landau, E. M. Lifshitz, and L. P. Pitaevskiĭ, *Statistical Physics, Part 1*, vol. 5 of *Course of theoretical physics*. Pergamon Press Ltd., 3 ed., 1980.
45. F. Gantmacher, *The Theory of Matrices*. Chelsea Publishing Company, 1959.
46. B. Craven, "Complex symmetric matrices," *J. Austral. Math. Soc.*, vol. 10, pp. 341–354, 1969.
47. O. Merchiers, F. Moreno, F. Gonzalez, and J. M. Saiz, "Light scattering by an ensemble of interacting dipolar particles with both electric and magnetic polarizabilities," *Phys. Rev. A.*, vol. 76, no. 4, p. 043834, 2007.

48. A. M. Kern and O. J. F. Martin, "Pitfalls in the determination of optical cross sections from surface integral equation simulations," *IEEE Trans. Ant. Prop.*, vol. 58, no. 6, pp. 2158–2161, 2010.
49. B. Hopkins, A. N. Poddubny, A. E. Miroshnichenko, and Y. S. Kivshar, "Circular dichroism induced by Fano resonances in planar chiral oligomers," *Laser Photon. Rev.*, vol. 10, no. 1, pp. 137–146, 2016.
50. C. Forestiere, L. D. Negro, and G. Miano, "Theory of coupled plasmon modes and Fano-like resonances in subwavelength metal structures," *Phys. Rev. B*, vol. 88, p. 155411, 2013.
51. M. Frimmer, T. Coenen, and A. F. Koenderink, "Signature of a Fano Resonance in a Plasmonic Metamolecule's Local Density of Optical States," *Phys. Rev. Lett.*, vol. 108, p. 077404, 2012.
52. A. Lovera, B. Gallinet, P. Nordlander, and O. J. Martin, "Mechanisms of Fano Resonances in Coupled Plasmonic Systems," *ACS Nano*, vol. 7 (5), pp. 4527–4536, 2013.
53. B. Hopkins, D. S. Filonov, S. B. Glybovski, and A. E. Miroshnichenko, "Hybridization and the origin of Fano resonances in symmetric nanoparticle trimers," *Phys. Rev. B*, vol. 92, p. 045433, 2015.
54. W. D. Heiss, "Exceptional points of non-hermitian operators," *J. Phys. A: Math Gen.*, vol. 37, p. 2455, 2001.
55. C. Dembowski, H.-D. Graf, H. L. Harney, A. Heine, W. D. Heiss, H. Rehfeld, and A. Richter, "The physics of exceptional points," *Phys. Rev. Lett.*, vol. 86, pp. 787–790, 2001.
56. W. D. Heiss, "The physics of exceptional points," *J. Phys. A: Math. Theor.*, vol. 45, p. 444016, 2001.
57. J. Yan, P. Liu, Z. Lin, H. Wang, H. Chen, C. Wang, and G. Yang, "Directional Fano resonances in a silicon nanoparticle dimer," *ACS Nano*, vol. 9, pp. 2968–2980, 2015.
58. R. M. Bakker, D. Permyakov, Y. F. Yu, D. Markovich, R. Paniagua-Domínguez, L. Gonzaga, A. Samusev, Y. Kivshar, B. Luk'yanchuk, and A. I. Kuznetsov, "Magnetic and electric hotspots with silicon nanodimers," *Nano Lett.*, vol. 15, no. 3, pp. 2137–2142, 2015.
59. U. Zywietz, M. K. Schmidt, A. B. Evlyukhin, C. Reinhardt, J. Aizpurua, and B. N. Chichkov, "Electromagnetic resonances of silicon nanoparticle dimers in the visible," *ACS Photon.*, vol. 2, pp. 913–920, 2015.
60. A. E. Miroshnichenko, B. Luk'yanchuk, S. A. Maier, and Y. S. Kivshar, "Optically induced interaction of magnetic moments in hybrid metamaterials," *ACS Nano*, vol. 6, no. 1, pp. 837–842, 2011.
61. I. Fernandez-Corbaton and G. Molina-Terriza, "Role of duality symmetry in transformation optics," *Phys. Rev. B*, vol. 88, p. 085111, 2013.
62. X. Zambrana-Puyalto, I. Fernandez-Corbaton, M. L. Juan, X. Vidal, and G. Molina-Terriza, "Duality symmetry and Kerker conditions," *Opt. Lett.*, vol. 38, no. 11, pp. 1857–1859, 2013.
63. A. E. Miroshnichenko and Y. S. Kivshar, "Fano resonances in all-dielectric oligomers," *Nano Lett.*, vol. 12, pp. 6459–6463, 2012.
64. D. S. Filonov, A. P. Slobozhanyuk, A. E. Krasnok, P. A. Belov, E. A. Nenasheva, B. Hopkins, A. E. Miroshnichenko, and Y. S. Kivshar, "Near-field mapping of Fano resonances in all-dielectric oligomers," *Appl. Phys. Lett.*, vol. 104, p. 021104, 2014.

List of Symbols

Symbol	Description
α, $\bar{\alpha}$	scalar and tensor dipole polarizabilities
c_0	speed of light in the background
ϵ_0, μ_0	background permittivity and permeability
$\bar{\epsilon}$	relative permittivity tensor
$\mathbf{E}$, $\mathbf{H}$	electric and magnetic field vectors
$\bar{G}_0$	dyadic Green's function
$\mathbf{J}$	electric current vector
k, $\mathbf{k}$	wavenumber and wavevector
λ, Λ	eigenvalues
$\mathbf{p}$, $\mathbf{m}$	electric and magnetic dipole moment vectors
σ_e, σ_s, σ_a	extinction, scattering and absorption cross-sections
$\bar{\chi}$, $\bar{\sigma}$	dielectric susceptibility and conductivity tensors
ω	angular frequency

Index